Published in final edited form as:
Contrast Media Mol Imaging. 2014 ; 9(1): 13–25. doi:10.1002/cmmi.1571.

Multicolor Computed Tomographic Molecular Imaging with Non-crystalline High Metal Density Nanobeacons

Dipanjan Pan[1,ǂ], **Carsten O. Schirra**[1], **Samuel A Wickline**[1], and **Gregory M Lanza**[1]

[1]Department of Medicine, Washington University School of Medicine, St Louis, MO 63108 and Philips Medical System, Briarcliff, NY

Abstract

Computed tomography (CT) is one of the most frequently pursued radiology technologies applied in the clinics today and in the preclinical field of biomedical imaging. Myriad advancement has been made to make this technique more powerful with improved signal sensitivity, rapid image acquisition and faster reconstruction. Synergistic development of novel nanoparticles has been adopted as the next generation CT contrasts agents for imaging specific biological markers. Nanometer-sized agents are anticipated to play a critical part in the prospect of medical diagnostics owing to their capabilities of targeting specific biological markers, extended blood circulation time and defined biological clearance. This review paper introduces the readers to the fundamental design principles of nanoparticulate CT contrast agents with a special emphasis on the molecular Imaging with non-crystalline high metal density nanobeacons.

Keywords

Computed tomographic imaging; nanoparticle; iodine; bismuth; gold; ytterbium; tantalum; fibrin; angiogenesis; sentinel lymph node; thrombus

1. Introduction

Molecular imaging offers a noninvasive approach to cellular and subcellular imaging, which was previously a functionality exclusively within the dominion of optical microscopes only a decade or so ago. Advancements in chemistry, molecular biology, genetics and engineering have created unprecedented cross-disciplinary collaborations driving clinical imaging strategies from gross anatomical to biochemical based assessments. This wave of research promises earlier diagnosis and more effective personalized treatment of intractable diseases than has heretofore been possible. [1–4]

Common clinical anatomical imaging modalities in use today are computed tomography (CT), magnetic resonance (MR) imaging, and ultrasonography (US). [5] Of these, CT is among the most attractive diagnostic tools in terms of its power to tomographically scan

Address correspondence to: Dipanjan Pan, PhD, Assistant Professor in Medicine, Division of Cardiology, Campus Box 8215, 660 Euclid Ave, Washington University School of Medicine, St. Louis, MO 63108, Tel: 314-454-7674, Fax: 314-454-5265 dipanjan@wustl.edu.
ǂPresent address: Department of Bioengineering, University of Illinois at Urbana-Champaign, dipanjan@illinois.edu

large portions of a body quickly. Unfortunately, CT has very little soft-tissue contrast and from a targeted molecular imaging perspective, the modality is relatively insensitive to probe detection when compared to the other modalities, particularly nuclear imaging. New nanoparticle chemistries for CT molecular imaging have recently been developed that have very high intrinsic metal density in order to achieve X-ray detectable concentrations. [6] For example, in case of targeted molecular imaging application, typically MRI requires a payload of 100,000 paramagnetic metal atoms per particle (~200 nm). As a direct comparison, the same biological target could be detected with CT only if a payload of ≥500,000 heavy metal atoms per nanoparticle is administered. Fortunately, the advancements in chemistry have been mirrored by parallel improvements in rapid image acquisition and statistically-based iterative reconstruction algorithms, the latter of which has reduced the imaging noise-floor allowing vastly more sensitive contrast detection than previously possible with traditional back project reconstruction routines. [7–8]

CT instrumentation has gone through a generational development over the last several years, with expansion of simultaneous slice numbers from 1 up to 320 simultaneous slices, to the more recent clinical introduction of dual-energy detector, kVp switching, the preclinical emergence of phase-contrast X-ray imaging and fluorescent CT imaging. Of particular interest has been the introduction of Spectral CT imaging based on K-edge detection, which should not be confused with SPECT/CT (a hybrid single photon emission computed tomography and computed tomography instrument). [9–10] Spectral or ‘multicolor’ CT can detect certain elements within the x-ray bandwidth based on their distinctive K-edge energies while simultaneously acquiring a traditional CT image. [11] The K-edge energy of an element is defined by the sudden increase in the attenuation coefficient of photons occurring at an energy exceeding the binding energy of the K shell electron of the atoms within the X-ray beam. (Figure 1)

In K-edge imaging, high accumulations of targeted elements bound to pathologic biomarkers can be presented on the typical CT image as colorized voxels. These regions of high attenuation voxels are readily differentiated from other attenuating sources, such as calcium deposits, which have distinctly lower K-edge energies. Moreover, regions of attenuation by K-edge metals can be known quantitatively from the photon counts. While conventional CT provides information about the overall attenuation of the emitted x-ray beam, photon-counting detectors retrieve spectral information across the bandwidth of the emitted photons. One of the immediate clinical applications of Spectral CT is in the cardiovascular area wherein CT molecular imaging of intracoronary micro thrombus associated with ruptured plaque must discriminate potential false-positive contrast signal derived from intraplaque calcium deposits to properly diagnose patients presenting to emergency departments with chest pain. [8–11]

2. Contrast agents: the fundamentals

Contrast materials containing high-atomic-number (Z) elements that absorb x-rays are of particular interest. Iodine has been widely used in the clinic as a blood pool CT contrast agent, in part because of attenuation attributable to its atomic number and because the rich abundance of photons within an X-ray beam of appropriate energy to induce additional K-

edge based attenuation in the compound. Barium (barium sulfate), an insoluble white powder, has a very high atomic number offering strong inherent attenuation with a K-edge energy value near the top of the X-ray beam bandwidth. Iodine is commonly used for CT blood pool imaging which bismuth compounds have been routinely used to assess digestive track anatomy and functionality. In terms of k-edge imaging, the commonly used iodinated contrast agents will unlikely to be useful for clinical applications due to its relatively low K-edge energy (I= 33 keV; Ba= 37keV), the impact of X-ray beam hardening (absorption of lower energy photons), and omnidirectional X-ray scattering incurred with patients. As a result, there is renewed interest in the development of engineered nanomaterials as CT contrast agents incorporating other high atomic number metals. [12] Examples of other high-atomic-number metals are gold (Au), gadolinium (Gd), bismuth (Bi) and tantalum (Ta). Myriad of advancements have been made on the development of nanoparticles for specific CT molecular imaging applications. These agents must show excellent radio-opacity, outstanding biocompatibility, in vivo stability (i.e., particular during circulatory transit to targets and through the imaging period), and desirable synthetic processing attributes, specifically tolerance to sterilization and prolonged shelf-life stability.

Although blood pool contrast agents maybe small molecular weight compounds, such as chelated metal complexes (Gd-DTPA or Yb-DTPA), [13–14] functionalizing such compounds with homing ligands would fail to bring adequate metal for CT detection to a site of interest. Therefore molecular imaging for CT requires the high mass delivery of high atomic weight elements, typically packaged into a nanoscale particle. Examples of “nano”-contrast agents include different classes of gold nanoparticles of varying size and morphology (spherical vs. rod, cages); gadolinium nanoparticles, ytterbium-based agents and tantalum-encapsulated nanometric agents.

3. Metal Nanoparticles

Developing nano particulate contrast agents with prerequisite properties for CT imaging continues to be a challenge. The insensitivity of X-ray-based techniques mandates the use of very high radio-opaque materials with very high metal densities. Such agents must be stable on the shelf for years and after IV administration, in the blood circulation for hours. Moreover, the radio-opaque material must be resistant to biometabolism or transmetallation loss of the metal in vivo, and the metal must undergo complete bioelimination in a reasonable period, after systemic use. Prevalent within the nano material science research community have been the study of “hard” crystalline metal nanoparticles. [12] These materials offer great physico-chemical properties, making them attractive candidate for CT contrast agents. The atomic number of the recently proposed metals gold, bismuth, gadolinium and tantalum is higher than that of the clinically used elements iodine or barium. As such, these metals offer stronger x-ray attenuation and much CT contrast. [6, 12] Moreover, the surface of the metal nanoparticles typically has strong binding affinity towards reactive groups e.g. thiol, disulfide amines etc. allowing for facile modification with biologically relevant molecules for targeting or drug delivery. [1]

A number of nanoparticulate contrast agents based on metallic nanocrystals for CT have been described recently. [6,12] While particles based on heavy-metal crystals (oxides,

sulfides etc.) are generally resistant to bio-metabolism, they are also not biologically eliminated. Core crystals size plays a determinant role in vivo pharmacokinetics, biodistribution, and bioelimination. Nanocrystals with size ranges higher than 10 nm, possibly >6nm, exceed the renal elimination threshold for urine excretion. Moreover, except in rodents with permissively open biliary canaliculi, hepatic elimination of these “hard” particles through bile is precluded, which may present regulatory challenges when trying to prove longterm safety.

Very recently, the design of colloidal “soft” nanoparticles that avoid the utilization of larger metal crystals, have been described. In this novel approach, noncrystalline organically soluble radio-opaque metallic small molecule agents (organometallics or metal complexes) or small nanoparticulates (<6 nm) are concentrated within a bigger nanoparticulate, stabilized by amphiphilies (e.g. diblock copolymers or phospholipid surfactant). [15] High biocompatibility of these agents is derived from the use of Generally Recognized As Safe (GRAS) quality components such as lipids, vegetable oil etc. [16] Exclusion of larger metallic crystalline particles ensures the rapid clearance of the residual metals following natural biliary renal excretion mechanisms. The use of lipids as outer coatings offers high biocompatibility as well as myriad chemical modification approaches to achieve homing and drug delivery functionalization. [1]

3.1. Nanoparticles incorporating bismuth

Rabin et al. reported polyvinyl pyrolidone-coated Bi_2S_3 nanoparticles (~50 nm). [17–18] Clear delineation and signal enhancement (HU=560) of the cardiac ventricles and major arterial and venous structures were seen in rats. Despite their long circulation time (>2 h) and adequate sensitivity in vivo, their long-term safety and clinical translatablity is questionable. These particles were based on heavy-metal crystals with size ~50+ nm, which would preclude substantive in vivo clearance. As these are preclinical research concepts, long-term safety studies and toxicity evaluation have and likely will not be pursued.

Pan et al. designed and developed radio-opaque colloidal nanoparticles utilizing the incorporation of small molecule organic-metal complexes at high density in lieu of large metal crystals. [16] They reported the synthesis of bismuth-incorporated NanoK and achieved the requisite high metal content (>500,000/NP) with a low-molecular-weight organo soluble bismuth complex (Figure 2). NanoK’s outer membrane comprised of phospholipids and can easily be functionalized for a variety of intravascular targets, such as. ligand-directed homing to fibrin of micro thrombus in coronary ruptured plaque. In this application, the selectivity of homing is assisted by particle-size (~200 nm), which constrains the agent to the vasculature during early circulation and imaging and prevents interaction with off-target intramural fibrin from within healed atherosclerotic plaque intramural haemorrhages. The NanoK particle incorporates bismuth neodecanoate at 40–70□% element v/v within a sorbitan sesquioleate core matrix. Phospholipid-encapsulated NanoK has a hydrodynamic diameter between 180 and 250 nm with a negative electrophoretic potential ranging from −20 to −27 mV. These particles were found to be suitable for K-edge coronary imaging where distinguishing the high attenuation of plaque calcium from fibrin-targeted contrast signal is essential.

As an example concept experiment, biotinylated NanoK or the control nanocolloid (i.e., no bismuth, ConNC) were pretargeted in vitro to acellular fibrin clots using a classic avidin–biotin coupling technique along with a well-characterized fibrin-specific monoclonal antibody (NIB5F3). [16] K-edge images of targeted fibrin clot samples seen in derived 3D maximum intensity projection reconstructions (Figure 3f) showed excellent signal enhancement from the bismuth-enriched fibrin clot surface (Figure 2d), whereas the control clot (top) exposed to targeted nonmetallic nanoparticles had negligible contrast, revealing only the highly attenuating calcium. The nominal size of NanoK, precluded deep penetration into the tight weave of fibrin fibrils, which is consistent with prior examples in this phantom model. The NanoK layer bound on the surface of the clots was 1 to 2 voxels (100 μm × 100 μm × 100 μm) thick with an average density of 3.5 mass% of bismuth for a layer thickness of 100 μm.

The feasibility of detecting fibrin at it physiological density as presented by unstable human atherosclerotic vascular tissue was tested in carotid artery endarterectomy (CEA) specimens. Microscopic fibrin deposits in CEA were exposed in vitro to fibrin-specific NanoK. Classic CT images (combination of photo effect, Compton and bismuth) of CEA tissue exposed to fibrin-targeted NanoK or ConNC revealed heavy calcification of both specimens, with no differentiation of the NanoK particles from the calcium based solely on X-ray attenuation. K-edge imaging distinguished the bound fibrin-targeted NanoK (color: gold) at 90.5 keV from the complicating calcium signal (color: red) at 4.0 keV. (Figure 4)

The in vivo sensitivity of NanoK was tested in a rabbit thrombus model. A balloon overstretch injuryinduced thrombus was formed within the iliac artery of an atherosclerotic rabbit. Anti-fibrin monoclonal antibody coupled directly to NanoK particles was incubated in situ with the thrombus over 30 min followed by a one hour washout into the open circulation. Figure 4b shows the reconstructed intra-arterial thrombus enhanced with fibrin-bound NanoK with spectral CT. The partial-occlusive thrombus formed within a 1.41 mm diameter artery, which was comparable to a small coronary artery in humans. Spectral CT was able to clearly differentiate bismuth signal from NanoK and the pathology within the vessel from the attenuation effects of bone. K-edge image and the traditional CT image were simultaneously acquired (Figure 4), which points towards the huge potential of the technique in a clinical setting.

Heavy metals used for CT imaging must be cleared from the body in a reasonably short time period. The whole-body bio-elimination of NanoK bismuth following intravenous injection was monitored in mice and analyzed using ICP-MS. In a two-week study, nearly all of the metal was cleared from the mice (Figure 5d), and >98% within 7 days. These data illustrate the concept that the high metal payload of NanoK will be bioeliminated within a reasonable short timeframe. Residual biodistribution of NanoK was studied on day 14 into primary clearance organs, (i.e., liver, spleen, kidney). Analytical survey with ICP revealed less than 10 ppb□mL^{-1} below the statistically valid lower detection limit of the instrument and method.

3.2 Nanoparticles incorporating gold

Gold nanoparticles absorb X-rays strongly and produce secondary electrons and photons that can kill surrounding cells, such as cancer cells. Additionally, gold (Au, 79) with its higher atomic number and higher absorption coefficient (at 100 keV: gold, 5.16 $cm^2\ g^{-1}$ vs. iodine, 1.94 $cm^2\ g^{-1}$) versus iodine (I, 53) provides about 2.7 times greater X-ray contrast per unit weight. This is particularly notable at the higher X-ray tube voltages, i.e. 90 KV, 120 and 140 kV, used in medical imaging. Additionally, gold nanoparticles, offer excellent safety profiles as well as the ability to be functionalized to target tissues of medical interest, but this advantage can be reversed for particles less than 2nm, which have unique chemical reactivity, or negated through surface coatings and charge. [19] Conversely, large particles of gold, greater than 10 nm appear inert and safe in cell cytotoxicity studies but their lack of bioelimination in humans pose long-term safety questions. Moreover, the crystalline structured form of large gold nanoparticles may compromise the validity of comparisons with other forms of medical gold, such as gold sodium thiomalate for rheumatoid arthritis, which has long fallen into disfavor due to myriad side-effects. Gold can transform absorbed light into heat, resulting in localized temperature rises, which has recently been used to provide contrast for photoacoustic imaging or for photothermal therapy. [20]

The majority of the gold synthetic protocols are based on chemical reduction methods in aqueous and non-aqueous media. In one method pioneered by Turkevich, gold chloride is reduced with sodium citrate in aqueous solution at boiling temperature to produce a citrate-capped particle. [21] The particle sizes can be varied from 15–150 nm by controlling the ratio of the reducing agent. To render them stable in saline solutions, these particles are coated with biocompatible organic or inorganic molecules e.g. polyethylene glycol (PEG), silica, lipids, bovine serum albumin (BSA) and different polymers. Different coating methods have been adopted e.g. ligand substitution, wrapping with amphiphiles or embedding in a carrier matrix. In the Brust-Schiffrin method, [22] a non-aqueous approach is followed to produce organically coated gold nanoparticles.

Xia et. al. invented a synthetic protocol for making gold nanocages following a galvanic replacement reaction. [23] In this method, Ag solid is used as a template for the reduction of $HAuCl_4$ due to their electrochemical potential difference to form Au atoms. In this reaction, the growth of AuNCs was templated over silver nanocubes that were concurrently produced. $3Ag\ (s) + AuCl_4^-(aq) \rightarrow Au\ (s) + 3Ag^+\ (aq) + 4Cl^-\ (aq)$. Ag nanocubes were derived using $AgNO_3$ or CF_3COOAg as a precursor to Ag, and a polyol reduction by using ethylene glycol as a solvent and a source of reducing agent. This reaction was further assisted with a capping agent, poly(vinyl pyrrolidone) (PVP). Subsequently, the addition of catalytic amounts of NaHS and or Cl^- ions imparted rapid nucleation of single-crystal seeds while simultaneously, due to oxidative etching, discarded twinned seeds, and ultimately formed single-crystal Ag nanocubes. Additional titration of these Ag nanocubes with $HAuCl_4$ was followed at 100°C in order to ensure maximal growth of thin layered Au on the surface of the Ag crystals and to evade precipitation of AgCl. Cooling the reaction precipitates AgCl, which was then dissolved in a saturated NaCl solution and eliminated, leaving AuNCs as the final remaining product. Other commonly pursued approaches to prepare gold nanoparticles involve ‘green’ approaches such as microwave and UV irradiation. [24–25]

Many laboratories have pursued research with gold nanoparticles:

- AuNPs have been conjugated to prostate-specific membrane antigen (PSMA) aptamers for targeting of PSMA on prostate cancer cells in vitro. In this work, Kim et al. was able to detect specific binding of the AuNPs with a clinical CT scanner. The therapeutic effect of doxorubicin-coupled to these particles was also evaluated in this model. [26]
- Alric et al. developed a dual modality probe from Au nanoparticles coated with a Gd chelate. [27] Direct comparison of both CT and MR images of a rat taken before and after administration of the Au/Gd nanoparticles showed enhancement in the kidneys, bladder and urine, which was corroborated ex vivo with inductively coupled Plasmon resonance mass spectrometric analyses of the excised tissues.
- Kopelman and coworkers synthesized gold nanorods (AuNR) and coupled them with UM-A9 antibodies for specifically targeting SCC head and neck cancer, and they elaborate on their research in a dedicated review in this special issue of the CMMI journal. [28] In this proof of principle experiment, the feasibility to identify the existence of SCC cancer cells, through CT scans was demonstrated. Gold nanoparticles were selectively homed to the targeted cancer cells yielding a strong selective X-ray attenuation that is distinct from the attenuation obtained from nontargeted cancer cells or by normal cells.
- In another example, lisinopril was used as a targeting moiety to prepare gold nanoparticle-based functional CT contrast agents following a ligand exchange reaction on citrate-coated gold nanoparticles. [29] Targeted gold nanoparticles assessed the targeting of angiotensin converting enzyme (ACE) using conventional CT. Clear enhancement was seen in the region of the lungs and heart, clearly indicating the targeting of ACE. ACE over expression is known to be associated with the development of cardiac and pulmonary fibrosis.
- Cormode et al., whose work is also highlighted in this CMMI journal issue, developed a gold highdensity lipoprotein nanoparticle contrast agent (Au-HDL) for characterization of macrophage burden, calcification, and stenosis of atherosclerotic plaques. [30] Spectral CT technique was employed to image these nanoparticles non-specifically accumulated in macrophages in atherosclerotic plaques. Multi color CT was able to distinguish the gold k-edge signal, iodine as a blood-pool contrast in vasculature, as well as calcified material (calcium phosphate), simultaneously and quantitatively. A preclinical spectral CT system (Philips Research, Hamburg) was used, in which incident x-rays were divided into six different energy bins for multicolor imaging. For atherosclerosis animal model, Apolipoprotein E knockout (apoE-KO) mice were. Gold nanoparticles were administered intravenously (500 mg/Kg). The blood pool iodinated contrast was injected 24 hours later followed by the Spectral CT imaging. Specific accumulation of the nanoparticles in macrophages was further confirmed by transmission electron microscopy and confocal microscopy and histopathology.

- Molecularly targeted gold nanobeacons (GNB) have been developed for Spectral CT imaging. Pan et al reported the synthesis of gold nanobeacons (GNB) by following a “particle within particle” approach. [31] In this procedure tiny 3–4 nm sized octanethiol-coated gold nanoparticles were concentrated (nominally 6,000 gold atoms/nanobeacons) within a bigger vascularly constrained nanoparticle (~120 nm), stabilized by phospholipids. The phospholipids mixture was comprised of phosphatidylcholine (PC, 91 mole %) and cholesterol (8 mole %) and included biotin-caproyl-PE (1 mole %) or a phospholipid anchored homing ligand (0.3 to 1.0 mole %) at the equimolar expense of PC dependent on the biological target under question. The GNB_1 particles were 154 ± 10 nm with polydispersity and zeta potential of 0.08 ± 0.03 and −47 ± 7 mV, respectively (Brookhaven Instrument Co.). Gold content, determined by ICP-MS, was 1080 μg/g of the 20% colloid suspension. By the virtue of the unique NIR optical properties of gold, these nanoparticles were successfully used for sensitive PAT imaging of atherosclerosis, sentinel lymph nodes and for the first time for detecting nascent sprouting angiogenic blood vessels. However, preliminary results with GNB particles produced poor contrast enhancement even in phantoms. The result was not unpredicted and it was quickly pointed out that for effective molecular imaging, nanoparticles designed for x-ray imaging must incorporate very high concentration of elements. Phantom studies indicated that at least 5×10^5 metal atoms per nanoparticle (e.g., gold atoms) for a 200nm agent is required for robust in vivo CT imaging.

Schirra et al reported the development of a second-generation gold nanobeacon (GNB_2), which incorporated at least five times more metal (nominally 580,000 gold atoms/beacons) than the previous generation. [32] The particles were synthesized similarly as lipid-encapsulated, vascularly constrained (>160 nm) nanobeacons incorporating tiny organically soluble oleate-coated gold nanoparticles (3–4 nm) within a polysorbate core. Higher metal loading was achieved by switching the core material from vegetable oil to polysorbate. (Figure 6) Transmission electron microscopy images revealed the presence of tiny gold particles encased within an outer lipid monolayer membrane. These particles had prolonged shelf-life stability at 4 °C. (Figure 7)

Initial in vitro imaging with GNB particles utilized fibrin clot phantoms and the aforementioned avidinbiotin coupling approach. The plasma clots were targeted with GNB_2 or the control nanocolloids (no gold) using a well-characterized fibrin-specific monoclonal antibody (NIB5F3) and placed in a tissue mimicking CT phantom. In a separate tube $CaCl_2$ (500 mM) was introduced to simulate arterial wall calcifications, a common feature of plaque complicating traditional CT coronary imaging applications. Additional $CaCl_2$ probes were included to introduce spectral attenuation effects that might be induced by the ribs and vertebra. Spectral CT readily detected the targeted GNB_2 bound to fibrin and distinguished it from the attenuation signal produced by calcium. Further, the use of statistical image reconstruction, reviewed by Schirra et al in greater detail elsewhere in this special issue on CT molecular imaging, showed that high SNR could allow dose reduction and/or faster scan times. In an in vivo model for sentinel lymph nodes (SLN) detection, gold nanobeacons injected into the foot-pad of a mouse migrated to a draining flank node where the

accumulation produced a very strong Spectral CT signal which was easily resolved from skeletal contrast signal or interference. (Figure 8)

3.3. Nanoparticles incorporating ytterbium

The use of ytterbium as a CT contrast agent was first explored in 80s by Unger et al. who demonstrated that Yb is more radioopaque than equimolar concentration of iodine at 125 kVp. [33] Ytterbium-DTPA chelate, with an overall LD50 reported to be 10 mM/kg (1.73 g ytterbium/kg) in rats, was evaluated as effective for pulmonary angiography in dogs, a result subsequently corroborated independently in the same animal model. Krause et al. conducted a series of studies to determine the utility of a more kinetically stable ytterbium chelate, Yb-EOB-DTPA. [34–35] Excellent tolerability of the complex was observed in vitro (thromboplastin time, effect on erythrocytes) and in vivo (acute, neural, and cardiovascular toxicities) in rat and rabbit models. In a systematic comparative study of metal contrast enhancement, Zwicker et al. confirmed a decrease in the enhancement in the order of Gd (120 kV) > Gd (137 kV) > Yb (120 kV) > Yb (137 kV) > iodine (120 kV) > iodine (137 kV). [36] The specific enhancement of Gd was 40.8 (120 kV), of Yb 34.2 and of iodine 29.6 HU. The in vivo dynamic CT imaging in dog showed enhancement of the liver for all three elements in the order of 21 HU (Gd) to 19 HU (Yb) and 12 HU (iodine). Gd and Yb achieved higher aortal contrast enhancement than iodine (190 vs 157 HU).

Very recently Xing et al reported a simple bimodal imaging platform based on PEGylated NaYbF(4): Tm^{3+} nanoparticles for both CT and NIR-fluorescence bioimaging. [37] The as-designed nanoparticles were less than 20 nm in diameter and showed excellent in vitro and in vivo performances in the dualbioimaging, very low cytotoxicity and no detectable tissue damage when tested over a month. Due to its high X-ray absorption coefficiency the Yb^{3+} in the lattice of $NaYbF_4$:$Tm3^{+}$ nanoparticles helped to function as a promising CT contrast medium while providing excellent sensitizing performance to enhance NIRfluorescent emissions. The particles excreted mainly via feces in rodents, without detectable remnant in vivo; however, the biliary pathway is permissive to particles in rats and mice but not in humans, wherein the particles would have safety issues with bioelimination.

Liu et al. designed and synthesized a PEG-coated Yb_2O_3:Er nanoparticles suitable for both X-ray CT imaging and up-conversion imaging. Compared with routinely used an iodinated contrast agent (i.e. Iobitridol) in clinic, these particles showed significantly enhanced contrast at a clinical 120 kVp voltage. These PEG-UCNPs were facile to construct, possessed excellent stability against in vivo environment, and held long blood circulation time. Cell-cytotoxicity assay, hemolytic activity, and post-injection histology analysis suggested good biocompatibility, indicating the feasibilities of PEG-UCNPs for in vivo applications. By doping 5% Er(3+) into the nanoparticles, PEG-UCNPs presented a long-term stable and nearly single-band red up-conversion emission upon continuous irradiation with a 980 nm laser.[38]

Pan et al. reported a novel molecular imaging agent based on Yb designed for use with spectral CT. [39] The synthetic approach involved the use of organically soluble Yb(III) complex to produce nanocolloids of Yb of noncrystalline nature incorporating a high density of Yb (>500K/nanoparticle) into a stable metal particle. (Figure 9) The resultant particles are

constrained to vasculature (~200 nm) and are highly selective for binding fibrin in the ruptured atherosclerotic plaque. Nanoparticles exhibited excellent signal sensitivity, and the spectral CT technique uniquely discriminates the K-edge signal (60 keV) of Yb from calcium (bones). (Figure 10)

3.4. Nanoparticles incorporating tantalum

Bonitatibus et al. developed a water-soluble tantalum oxide-based CT contrast agent. [40] These nanoparticles were derived from Ta_2O_5, and were acutely chemically inert and with good biocompatibility. These nanoparticles (<6nm) were within the threshold range of renal clearance and were cleared from the blood within seconds following injection in rodents. In vivo study showed clear delineation of a rat's vena cava and abdominal aorta. Very recently, a pegylated version of similar particles were devised with a much improved blood circulation time of 3h within the hydrodynamic size range (5–15 nm, before PEGylation), but those agents with larger particle size will be challenged on the long-term safety/bioelimination front, which has become one of the most difficult biological barriers to overcome in this field. [41–42]

3.4. Other agents

Liposomes are classified as one of the most extensively studied carrier platforms comprising phospholipid vesicles with an internal aqueous phase and bilayer membrane structure comparable to that of a biological membrane. Liposomes have been incorporated with iodine molecules to form particulates in the size ranges from 100–500nm. They have demonstrated to have in vivo contrast and long blood circulation time (hours). One interesting example exploited the amphiphilic nature of the lipid bilayer and incorporated water-soluble iodinated compounds together with organo-soluble iodized oil. Kweon et al. reported this innovative approach to increase the iodine concentrations in the liposomes for robust in vivo CT imaging. [43] Despite these promises, the possibility to clinically translate a liposomal CT contrast is very poor since it involves careful preparation, complicated purification and relative instability in biological media.

Iodinated contrast molecules can be entrapped covalently or noncovalently to polymer chains. However, the fundamental requirement to incorporate heavy payload of iodine molecules makes it challenging to synthesize stable suspension of polymeric iodinated contrast agents. Particular attention must be paid to increase their shelf-life properties, prevent decomposition and agglomeration in vivo while maintaining their robust detection with x-ray imaging. Pan et al. recently reported the synthesis and characterization of a colloidal iodinated polymer nanoparticle (~200 nm) incorporating ethiodol stabilized by PS-b-PAA di block copolymer. [15] This report described a novel class of soft type, vascularconstrained, stable radio-opaque polymeric nanoparticle using organically soluble radio-opaque elements encapsulated by synthetic amphiphile. This agent offers several-fold CT signal enhancement in vitro and in vivo demonstrating detection sensitivity reaching down to the low nanomolar particulate concentration range. A similar approach has been followed by de Vries et al. to develop radiopaque iodinated emulsions with high iodine payload (130 mg I/ml) for blood pool CT imaging. This work demonstrated that

polymerstabilized particles remained stable similar to the lipid-stabilized emulsions in vivo. [44]

4. Conclusion and future of CT Imaging

CT is one of the most frequently pursued imaging techniques applied in the clinics today. Much advancement has been made to make this technique more powerful with improved signal sensitivity, rapid image acquisition and faster reconstruction. New multidetector cardiac CTs (MDCT) can image the heart within the span of a few beats, and as such, it is the favored noninvasive approach to assess coronary anatomy rapidly. However, MDCT has proven to be more useful for excluding coronary disease than for making positive diagnoses. The newest advancement in CT imaging technology, Spectral (Multicolored) CT uniquely enhances traditional CT images, which are based on the photoelectric and Compton effects, with the capability to image and quantify certain metals based on distinctive K-edge values. Synergistic development of novel nanoparticles has been adopted as the next generation CT contrasts agents for imaging specific biological markers. Nanometer-sized agents are anticipated to play a critical part in the prospect of medical diagnostics owing to their capabilities of targeting specific biological markers, extended blood circulation time and defined biological clearance. We discussed the fundamental design principles of nanoparticulate CT contrast agents with a special emphasis on the molecular Imaging with non-crystalline high metal density nanobeacons. These metallic nanobeacons offer excellent signal sensitivity without comprising the biological safety. Spectral CT in combination of these molecularly targeted “soft” metal contrast agents can provide us quantitative information from the disease site, revealing not only the image of nanoparticle-enhanced pathology but also providing the amount of metal (i.e., the number of nanoparticles) bound in a given locality. It is critical to point out that although the sensivity of In the cardiovascular area, in the future, quantification of the extent of intraluminal plaque rupture may allow risk stratification of lesions demanding catheter-based stabilization protocol versus aggressive medical management of minor intimal ruptures expected to heal spontaneously. While spectral CT is still preclinical in nature, the growth of dual energy CT instruments within hospitals worldwide will offer a pre-installed base to pursue clinical studies when these metallic nanoagents reach clinical phase.

Acknowledgments

This was supported by NIH grant number U01 NS073457 - Characterization/bioinformatics-modeling of nanoparticle:complement interactions, R01 CA154737 - NEXT GENERATION APPROACHES TO BREAST CANCER USING IMAGE GUIDED DRUG DELIVERY, R01 HL113392 - Theranostic Approach to Asthma Using Anti-Angiogenic Nanomedicine, R01 HL073646 - ANTI-INFLAMMATORY THERAPEUTICS FOR CARDIOVASCULAR DISEASE; METHODS IN MOLECULAR IMAGING AND TARGETED THERAPEUTICS, R01 AR056468 - Targeted Nanotherapy in the Treatment of Inflammatory Arthriti U54 CA136398 - Photoacoustic / Optical / Ultrasonic Imaging of Sentinel Lymph Nodes and Metastas; Primary Project: SLN Mapping, R42 HL112518 - Targeted Nanoparticles of Bismuth Organo Complexes for Spectral CT Imaging of Cor

References

1. Pan D, Lanza GM, Wickline SA, Caruthers SD. Nanomedicine: perspective and promises with ligand-directed molecular imaging. Eur J Radiol. 2009; 70(2):274–285. [PubMed: 19268515]

2. Pan D. Theranostic nanomedicine with functional nanoarchitecture. Mol Pharm. Mar 4; 2013 10(3): 781–782. [PubMed: 23452025]
3. Jokerst JV, Gambhir SS. Molecular imaging with theranostic nanoparticles. Acc Chem Res. 2011; 44(10):1050–1060. [PubMed: 21919457]
4. Pysz MA, Gambhir SS, Willmann JK. Molecular imaging: current status and emerging strategies. Clin Radiol. 2010; 65(7):500–516. [PubMed: 20541650]
5. Kircher MF, Willmann JK. Molecular body imaging: MR imaging, CT, and US. part I. principles. Radiology. 2012; 263(3):633–643. [PubMed: 22623690]
6. Shilo M, Reuveni T, Motiei M, Popovtzer R. Nanoparticles as computed tomography contrast agents: current status and future perspectives. Nanomedicine (Lond). 2012; 7(2):257–269. [PubMed: 22339135]
7. Köhler T, Brendel B, Roessl E. Iterative reconstruction for differential phase contrast imaging using spherically symmetric basis functions. Med Phys. 2011; 38(8):4542–4545. [PubMed: 21928625]
8. Schirra C, Roessl E, Koehler T, Brendel B, Thran A, Pan D, Anastasio M, Proksa R. Statistical Reconstruction of Material Decomposed Data in Spectral CT. IEEE Trans Med Imaging. Mar 7.2013
9. Feuerlein S, Roessl E, Proksa R, Martens G, Klass O, Jeltsch M, Rasche V, Brambs HJ, Hoffmann MH, Schlomka JP. Multienergy photon-counting K-edge imaging: potential for improved luminal depiction in vascular imaging. Radiology. 2008; 249(3):1010–1016. [PubMed: 18849505]
10. Roessl E, Herrmann C, Kraft E, Proksa R. A comparative study of a dual-energy-like imaging technique based on counting-integrating readout. Med Phys. 2011; 38(12):6416–6428. [PubMed: 22149825]
11. Roessl E, Brendel B, Engel KJ, Schlomka JP, Thran A, Proksa R. Sensitivity of photon-counting based K-edge imaging in X-ray computed tomography. IEEE Trans Med Imaging. 2011; 30(9): 1678–1690. [PubMed: 21507770]
12. Liu Y, Ai K, Lu L. Nanoparticulate X-ray computed tomography contrast agents: from design validation to in vivo applications. Acc Chem Res. 2012; 45(10):1817–1827. [PubMed: 22950890]
13. Bloem JL, Wondergem J. Gd-DTPA as a contrast agent in CT. Radiology. 1989; 171(2):578–579. [PubMed: 2704827]
14. Zwicker C, Hering M, Langer R. Computed tomography with iodine-free contrast media. Eur Radiol. 1997; 7(7):1123–1126. [PubMed: 9265688]
15. Pan D, Williams TA, Senpan A, Allen JS, Scott MJ, Gaffney PJ, Wickline SA, Lanza GM. Detecting vascular biosignatures with a colloidal, radio-opaque polymeric nanoparticle. J Am Chem Soc. Oct 28; 2009 131(42):15522–15527. [PubMed: 19795893]
16. Pan D, Roessl E, Schlomka JP, Caruthers SD, Senpan A, Scott MJ, Allen JS, Zhang H, Hu G, Gaffney PJ, Choi ET, Rasche V, Wickline SA, Proksa R, Lanza GM. Computed tomography in color: NanoK-enhanced spectral CT molecular imaging. Angew Chem Int Ed Engl. 2010; 49(50): 9635–9639. [PubMed: 21077082]
17. Rabin O, Manuel Perez J, Grimm J, Wojtkiewicz G, Weissleder R. An X-ray computed tomography imaging agent based on long-circulating bismuth sulphide nanoparticles. Nat Mater. 2006; 5(2):118–122. [PubMed: 16444262]
18. Leung, K. Molecular Imaging and Contrast Agent Database (MICAD) [Internet]. Bethesda (MD): National Center for Biotechnology Information (US); Bismuth sulphide polyvinylpyrrolidone nanoparticles; p. 2004-2013.
19. Pan Y, Leifert A, Ruau D, Neuss S, Bornemann J, Schmid G, Brandau W, Simon U, Jahnen-Dechent W. Gold nanoparticles of diameter 1.4 nm trigger necrosis by oxidative stress and mitochondrial damage. Small. 2009; 5(18):2067–2076. [PubMed: 19642089]
20. Pan D, Pramanik M, Wickline SA, Wang LV, Lanza GM. Recent advances in colloidal gold nanobeacons for molecular photoacoustic imaging. Contrast Media Mol Imaging. 2011; 6(5):378–388. [PubMed: 22025338]
21. Kimling J, Maier M, Okenve B, Kotaidis V, Ballot H, Plech A. Turkevich method for gold nanoparticle synthesis revisited. J Phys Chem B. 2006; 110(32):15700–15707. [PubMed: 16898714]

22. Liz-Marzán LM. Gold nanoparticle research before and after the Brust-Schiffrin method. Chem Commun (Camb). 2013; 49(1):16–18. [PubMed: 23032158]
23. Xia Y, Li W, Cobley CM, Chen J, Xia X, Zhang Q, Yang M, Cho EC, Brown PK. Gold nanocages: from synthesis to theranostic applications. Acc Chem Res. 2011; 44(10):914–924. [PubMed: 21528889]
24. Dreaden EC, Alkilany AM, Huang X, Murphy CJ, El-Sayed MA. The golden age: gold nanoparticles for biomedicine. Chem Soc Rev. 2012; 41(7):2740–2779. [PubMed: 22109657]
25. Mieszawska AJ, Mulder WJ, Fayad ZA, Cormode DP. Multifunctional gold nanoparticles for diagnosis and therapy of disease. Mol Pharm. 2013; 10(3):831–847. [PubMed: 23360440]
26. Kim D, Jeong YY, Jon S. A drug-loaded aptamer-gold nanoparticle bioconjugate for combined CT imaging and therapy of prostate cancer. ACS Nano. 2010; 4(7):3689–3696. [PubMed: 20550178]
27. Alric C, Taleb J, Le Duc G, Mandon C, Billotey C, Le Meur-Herland A, Brochard T, Vocanson F, Janier M, Perriat P, Roux S, Tillement O. Gadolinium chelate coated gold nanoparticles as contrast agents for both X-ray computed tomography and magnetic resonance imaging. J Am Chem Soc. 2008; 130(18):5908–5915. [PubMed: 18407638]
28. Popovtzer R, Agrawal A, Kotov NA, Popovtzer A, Balter J, Carey TE, Kopelman R. Targeted gold nanoparticles enable molecular CT imaging of cancer. Nano Lett. 2008; 8(12):4593–4596. [PubMed: 19367807]
29. Ghann WE, Aras O, Fleiter T, Daniel MC. Syntheses and characterization of lisinopril-coated gold nanoparticles as highly stable targeted CT contrast agents in cardiovascular diseases. Langmuir. 2012; 28(28):10398–10408. [PubMed: 22702239]
30. Cormode DP, Roessl E, Thran A, Skajaa T, Gordon RE, Schlomka JP, Fuster V, Fisher EA, Mulder WJ, Proksa R, Fayad ZA. Atherosclerotic plaque composition: analysis with multicolor CT and targeted gold nanoparticles. Radiology. 2010; 256(3):774–782. [PubMed: 20668118]
31. Pan D, Pramanik M, Senpan A, Allen JS, Zhang H, Wickline SA, Wang LV, Lanza GM. Molecular photoacoustic imaging of angiogenesis with integrin-targeted gold nanobeacons. FASEB J. 2011; 25(3):875–882. [PubMed: 21097518]
32. Schirra CO, Senpan A, Roessl E, Thran A, Stacy AJ, Wu L, Proska R, Pan DJ. Mater Chem. 2012; 22(43):23071–23077.
33. Unger E, Gutierrez F. Ytterbium-DTPA. A potential intravascular contrast agent. Invest Radiol. 1986; 21(10):802–807. [PubMed: 3771152]
34. Krause W, Schuhmann-Giampieri G, Bauer M, Press WR, Muschick P. Ytterbium- and dysprosium-EOB-DTPA. A new prototype of liver-specific contrast agents for computed tomography. Invest Radiol. 1996; 31(8):502–511. [PubMed: 8854197]
35. Schmitz SA, Wagner S, Schuhmann-Giampieri G, Krause W, Bollow M, Wolf KJ. Gd-EOB-DTPA and Yb-EOB-DTPA: two prototypic contrast media for CT detection of liver lesions in dogs. Radiology. 1997; 205(2):361–366. [PubMed: 9356615]
36. Zwicker C, Langer M, Langer R, Keske U. Comparison of iodinated and noniodinated contrast media in computed tomography. Invest Radiol. 1991; 261(Suppl):S162–S164. [PubMed: 1808117]
37. Xing H, Bu W, Ren Q, Zheng X, Li M, Zhang S, Qu H, Wang Z, Hua Y, Zhao K, Zhou L, Peng W, Shi J. A NaYbF4: Tm3+ nanoprobe for CT and NIR-to-NIR fluorescent bimodal imaging. Biomaterials. 2012; 33(21):5384–5393. [PubMed: 22538199]
38. Liu Y, Ai K, Liu J, Yuan Q, He Y, Lu L. A high-performance ytterbium-based nanoparticulate contrast agent for in vivo X-ray computed tomography imaging. Angew Chem Int Ed Engl. 2012; 51(6):1437–1442. [PubMed: 22223303]
39. Pan D, Schirra CO, Senpan A, Schmieder AH, Stacy AJ, Roessl E, Thran A, Wickline SA, Proska R, Lanza GM. An early investigation of ytterbium nanocolloids for selective and quantitative "multicolor" spectral CT imaging. ACS Nano. 2012; 6(4):3364–3370. [PubMed: 22385324]
40. Bonitatibus PJ Jr, Torres AS, Goddard GD, FitzGerald PF, Kulkarni AM. Synthesis, characterization, and computed tomography imaging of a tantalum oxide nanoparticle imaging agent. Chem Commun (Camb). 2010; 46(47):8956–8958. [PubMed: 20976321]
41. Bonitatibus PJ Jr, Torres AS, Kandapallil B, Lee BD, Goddard GD, Colborn RE, Marino ME. Preclinical assessment of a zwitterionic tantalum oxide nanoparticle X-ray contrast agent. ACS Nano. 2012; 6(8):6650–6658. [PubMed: 22768795]

42. Torres AS, Bonitatibus PJ Jr, Colborn RE, Goddard GD, FitzGerald PF, Lee BD, Marino ME. Biological performance of a size-fractionated core-shell tantalum oxide nanoparticle x-ray contrast agent. Invest Radiol. 2012; 47(10):578–587. [PubMed: 22836312]

43. Kweon S, Lee HJ, Hyung WJ, Suh J, Lim JS, Lim SJ. Liposomes coloaded with iopamidol/lipiodol as a RES-targeted contrast agent for computed tomography imaging. Pharm Res. 2010; 27(7): 1408–1415. [PubMed: 20424895]

44. de Vries A, Custers E, Lub J, van den Bosch S, Nicolay K, Grüll H. Block-copolymer-stabilized iodinated emulsions for use as CT contrast agents. Biomaterials. 2010; 31(25):6537–6544. [PubMed: 20541800]

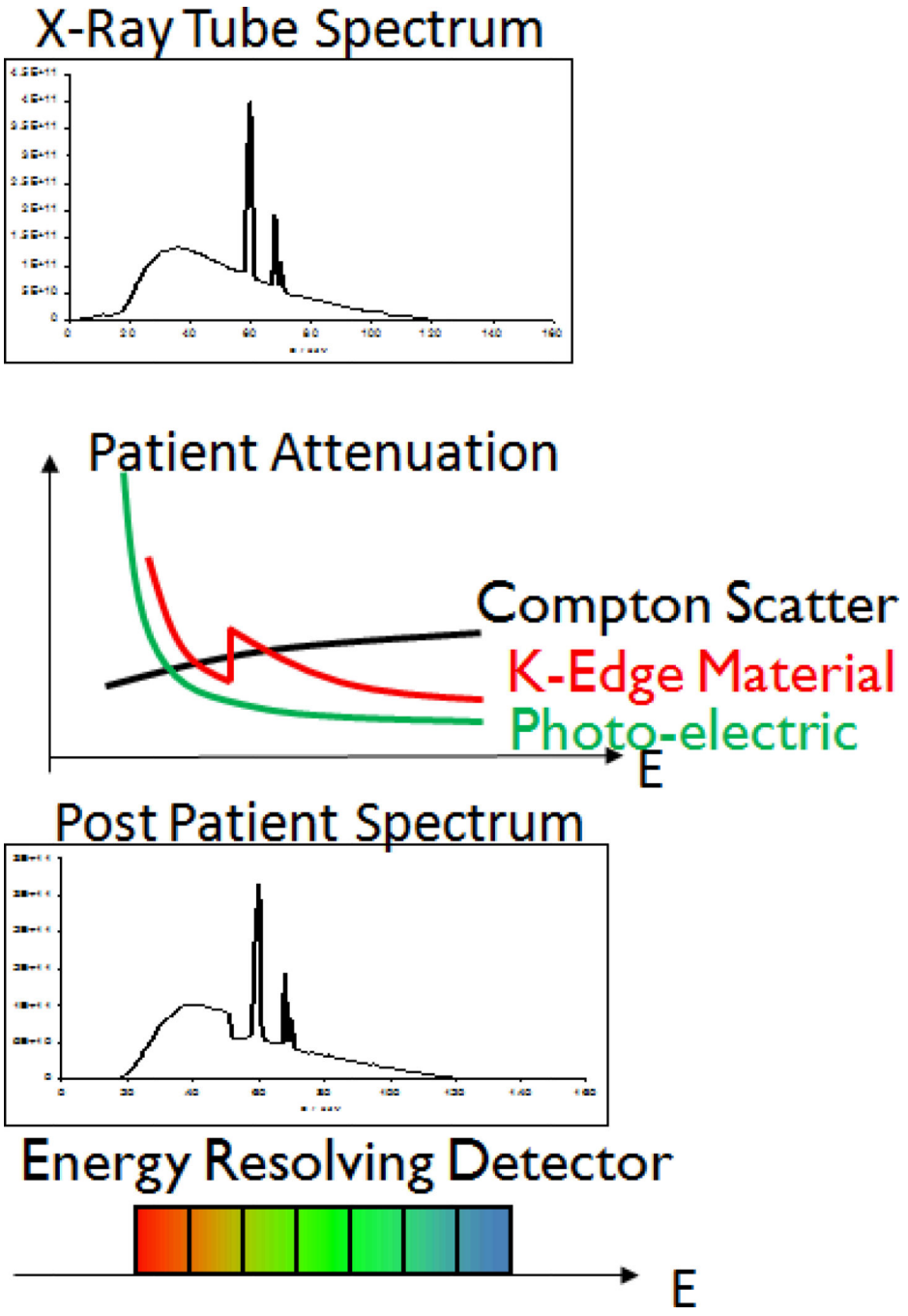

Figure 1.

Spectra for CT acquisitions with mean energy and relative photon flux transmission efficiency. Spectral or 'multicolor' CT can detect elements within the x-ray bandwidth based on their distinctive K-edge energies while simultaneously acquiring a traditional CT image. The K-edge energy of an element is defined by the sudden increase in the attenuation coefficient of photons occurring at an energy exceeding the binding energy of the K shell electron of the atoms within the X-ray beam.

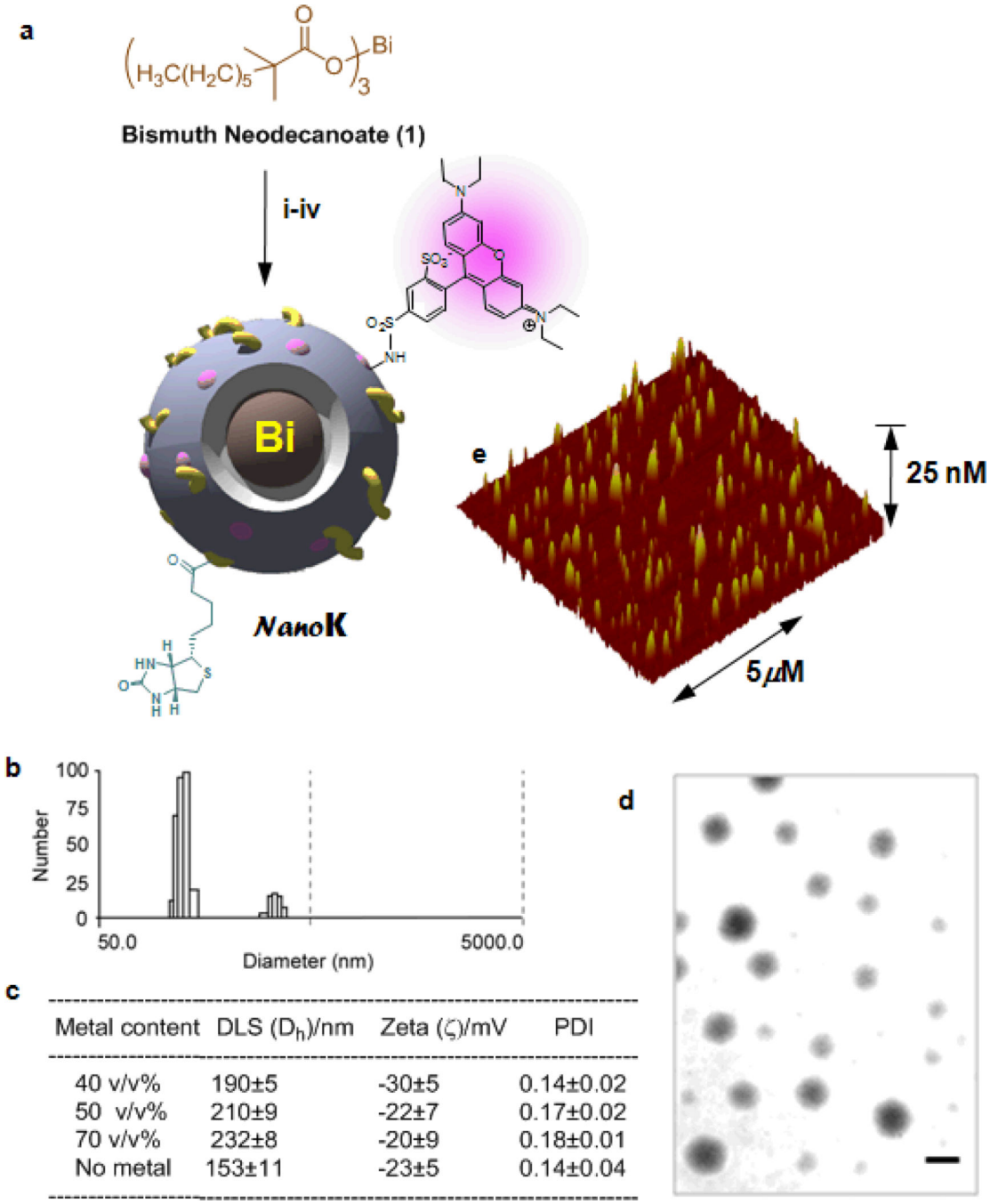

c

Metal content	DLS (D_h)/nm	Zeta (ζ)/mV	PDI
40 v/v%	190±5	-30±5	0.14±0.02
50 v/v%	210±9	-22±7	0.17±0.02
70 v/v%	232±8	-20±9	0.18±0.01
No metal	153±11	-23±5	0.14±0.04

Figure 2.

Synthesis and physico-chemical characterization of NanoK: (a) Schematic describing the preparation of bismuth-enriched K-edge nanocolloid (NanoK)): (i) Suspension of bismuth neodecanoate (1) in sorbitan sesquioleate, vigorously vortex and mixing, filter using cotton bed, vortex; (ii) preparation of phospholipid thin film (iii) resuspension of the thin film in water (0.2 μM); (iv) microfluidization at 4°C, 12,000 psi, 4 min, dialysis (cellulosic membrane, MWCO 20K).; (b)hydrodynamic particle size distribution from DLS; (c)

characterization table for three replicates of NanoK; (d) anhydrous state TEM images (staining: uranyl acetate; scale bar: 100nm; (e) AFM image

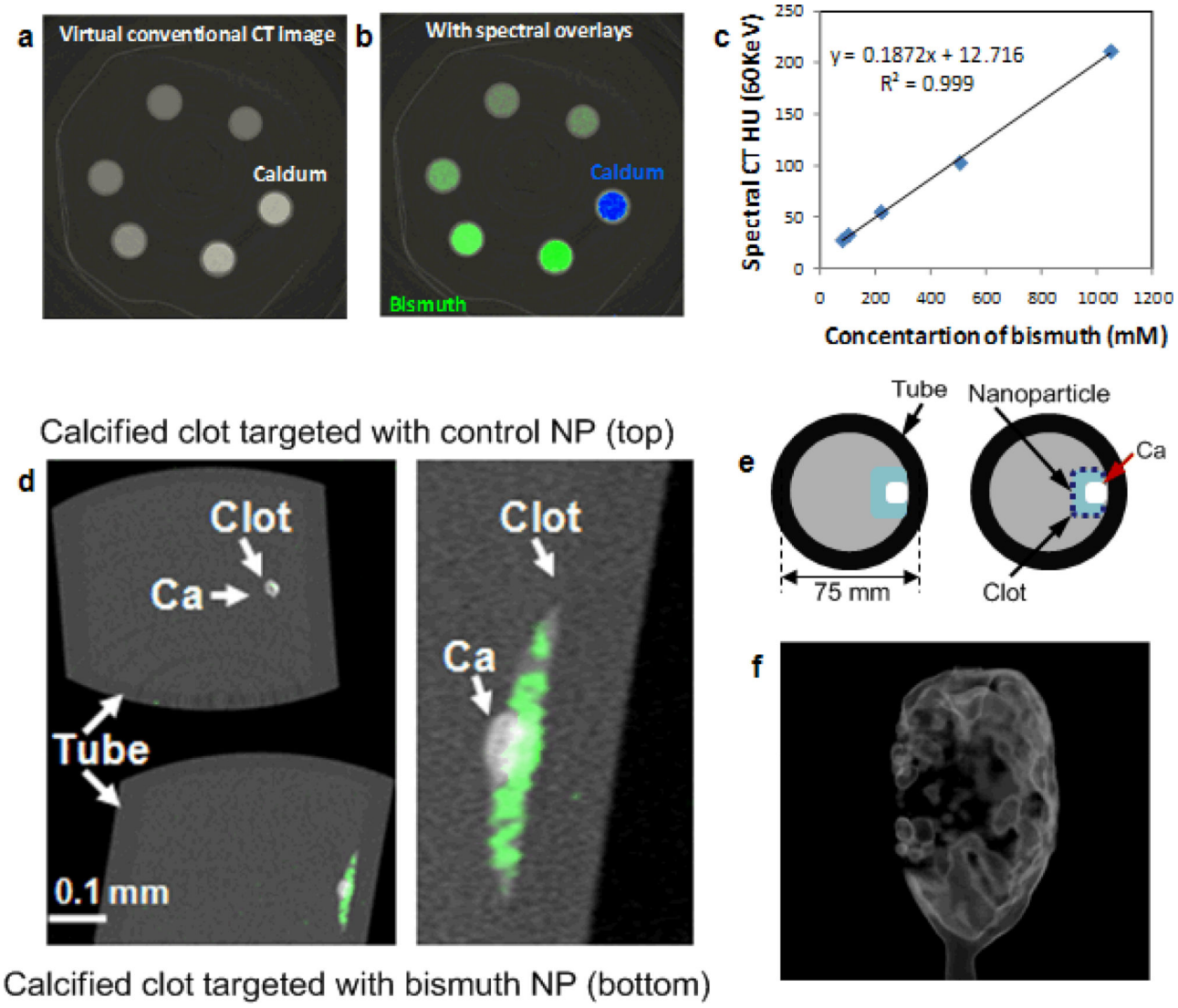

Figure 3.

Virtual conventional CT (a) and spectral CT (b) cross-sectional slices of serially diluted NanoK (green) and calcium (blue) phantoms; (c) variation of spectral CT signal (HU) with bismuth concentration; (d) cross-sectional slices of fibrin clot targeted with NanoK presenting calcium; (e) pictorial representation of the vessel phantom; (f) gradient rendered image of fibrin clot targeted with NanoK (Scale: 10 mm).

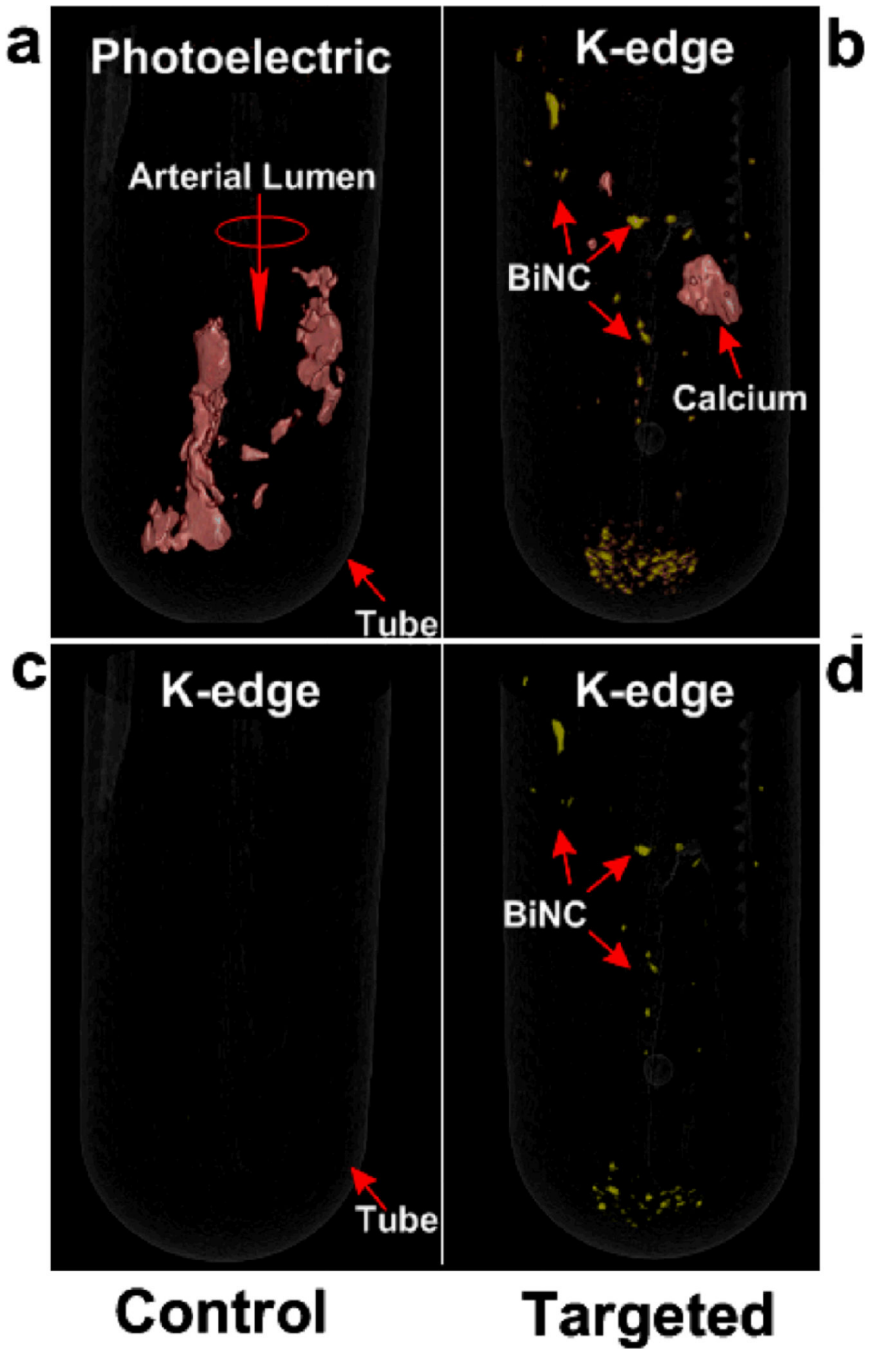

Figure 4.

(a) Photoelectric image of CEA specimen targeted with CoNC showing calcium (presented in red); (b) Spectral CT image of CEA specimen targeted with CoNC revealing no presence of the K-edge metal; (c) photoelectric image of CEA specimen targeted with NanoK showing but not differentiating the attenuation contrast of both plaque calcium and the fibrin-targeted NanoK; (d) Spectral CT image of CEA specimen after fibrin-targeted NanoK showing the spatial distribution and sparse concentration of thrombus remaining on human

carotid specimen. Note: Fibrin targeted NanoK signal at the bottom of the tube represents thrombus dislodged from CEA during processing.

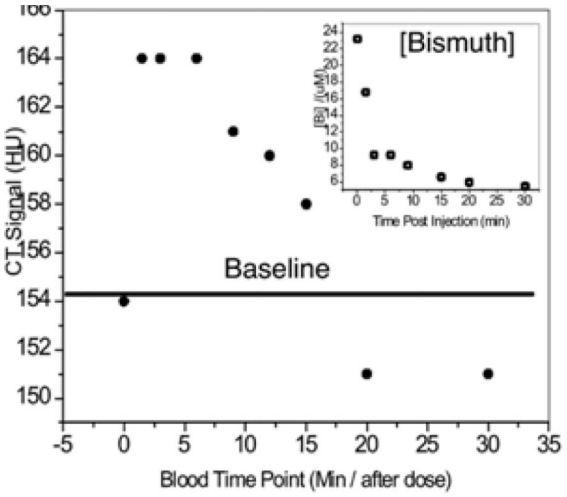

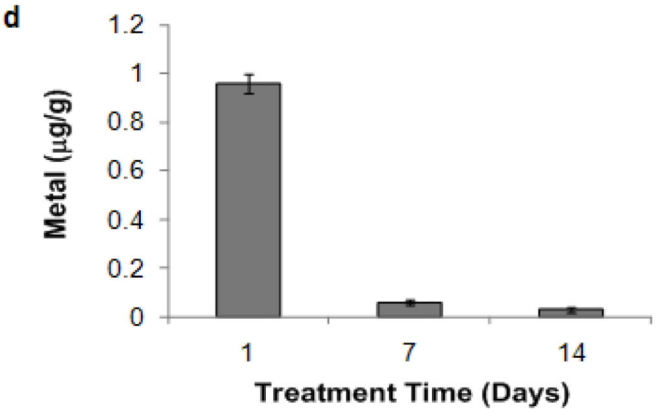

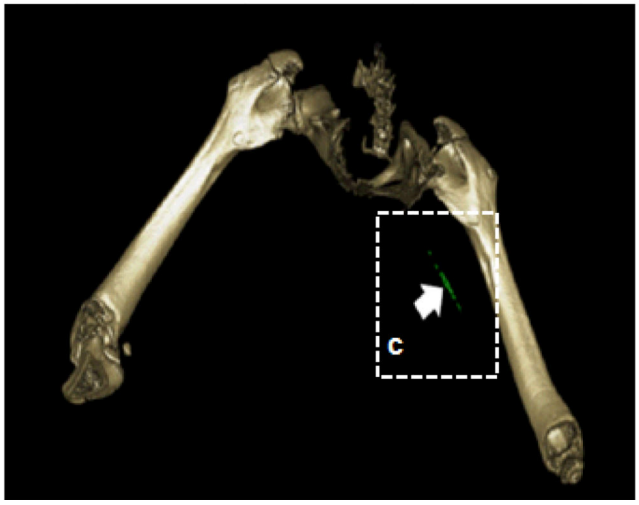

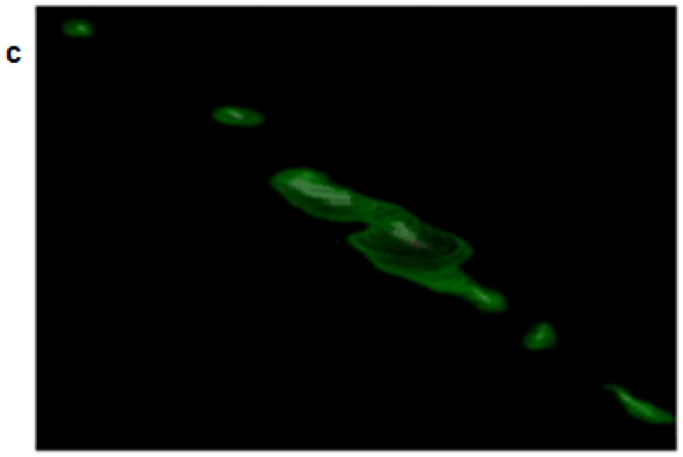

Figure 5.

(a) CT blood pool signal in rabbits following IV injection of NanoK. CT scan imaging parameters were thickness 0.8, increment 0.8, kv 90, mAs 1500, resolution HIGH, collimation 4×0.75, pitch 0.35, rotation time 1.5 seconds, FOV 75mm. Inset, The concentration of bismuth (ICP) in blood versus time post injection. Note that the background signal is at baseline in less than 30 minutes; (b–c) targeting in situ clot (thrombus) in rabbits; (d) two weeks clearance profile of bismuth from mice.

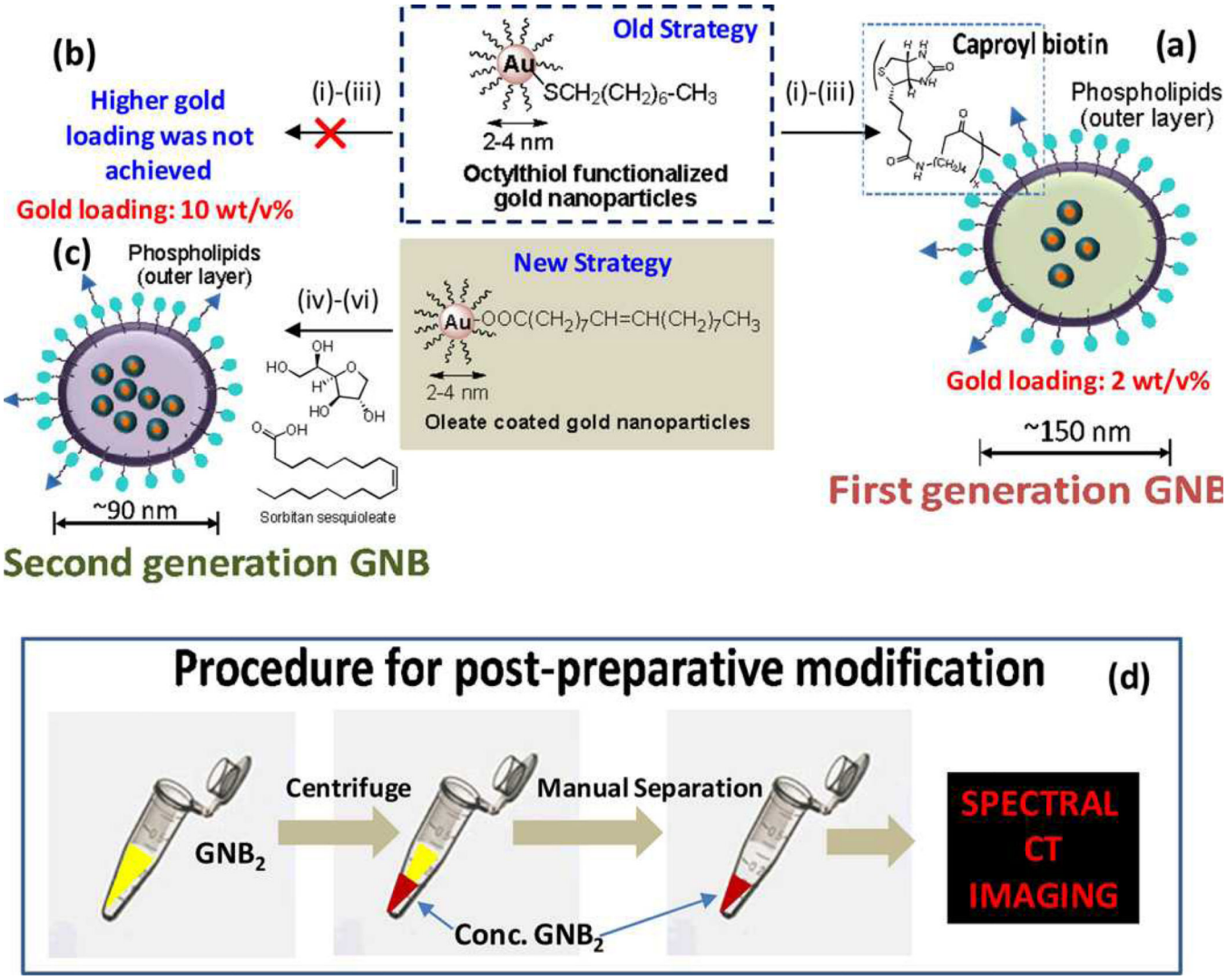

Figure 6.

Synthesis and post-preparative modification of GNB: (a) previous synthetic approach to first generation GNB particles from octanethiol coated AuNP with a final gold loading c.a. 2 w/v %: (i) gold nanoparticles suspended in vegetable oil, (ii) preparation of phospholipids thin film, (iii) microfluidization of gold nanoparticle-vegetable oil with surfactants in water; (b) new strategy to increase final gold loading up to 10 w/v%: oleate coated gold nanoparticles were suspended in sorbitan sesquioleate and microfluidized with phospholipids thin film mixture as a 2-0-20 formulation. reaction condition: (i) gold nanoparticles suspended in polysorbate, (ii) preparation of phospholipids thin film, (iii) microfluidization of gold nanoparticle-polysorbate with surfactants in water; 20,000 psi (141 MPa), 4°C, 4 min; (d) schematic representation of the procedure to concentrate GNB2 prior to spectral CT imaging.

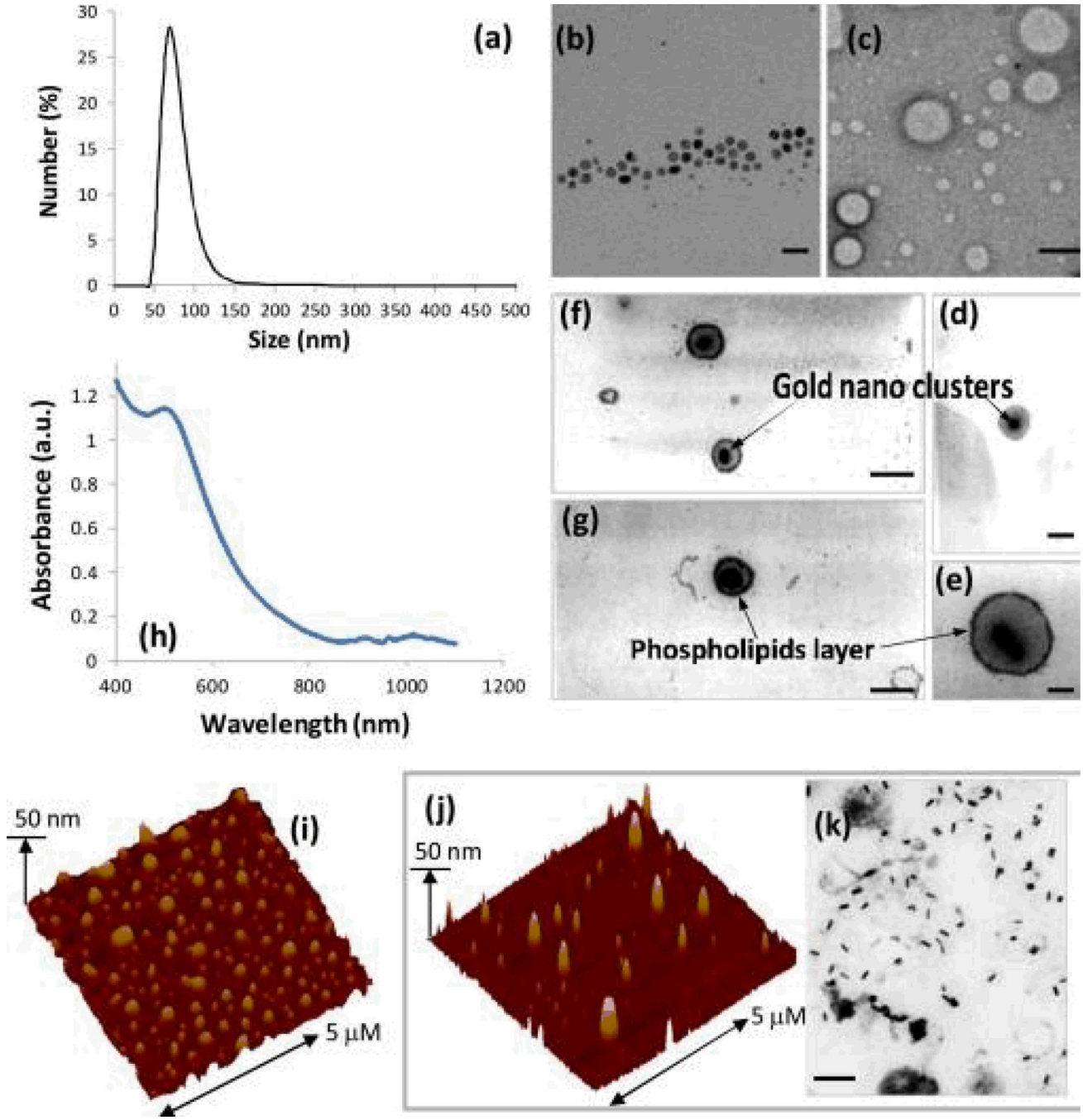

Figure 7.

Characterization of GNB: (a) number-averaged hydrodynamic diameter of GNB2 from dynamic light scattering measurements; TEM images of (b) oleate coated gold nanoparticles, scale bar= 20 nm, (c) control nanobeacons with no gold incorporated, scale bar= 100 nm, (d) first generation GNB (scale bar= 100 nm) and (e–g) second generation GNB revealing the gold clusters entrapped inside the phospholipids membrane (scale bar= 100 nm); (h) UV-vis spectrum of GNB2 in water confirming the presence of gold nanoparticle cluster and their surface plasmon resonance. AFM images of GNB2 (i) and

GNB (j, rod); (k) TEM image of GNB (rod) showing the presence of discrete gold rod nanoparticles of larger dimension within a phospholipids encapsulation (scale bar= 100 nm).

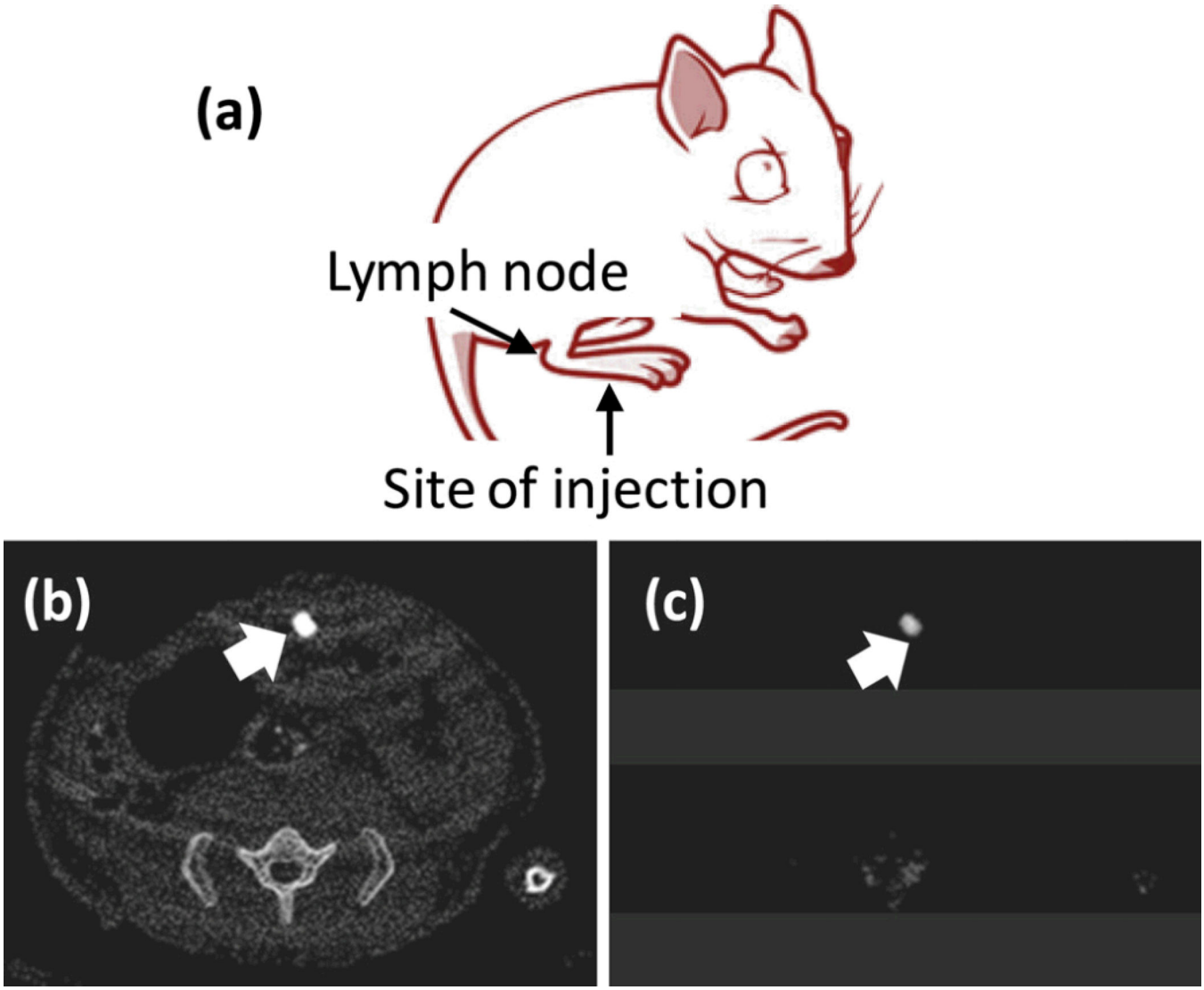

Figure 8.

In vivo noninvasive spectral CT imaging of sentinel lymph nodes. (a) A cartoon illustrating the site of injection and the area of interest. 150 μL of nanobeacons were injected intradermally in all the cases; (b) regional sentinel lymph nodes were clearly contrasted in conventional CT; (c) K-edge contrast of accumulated gold in the lymph node was selectively imaged with spectral CT.

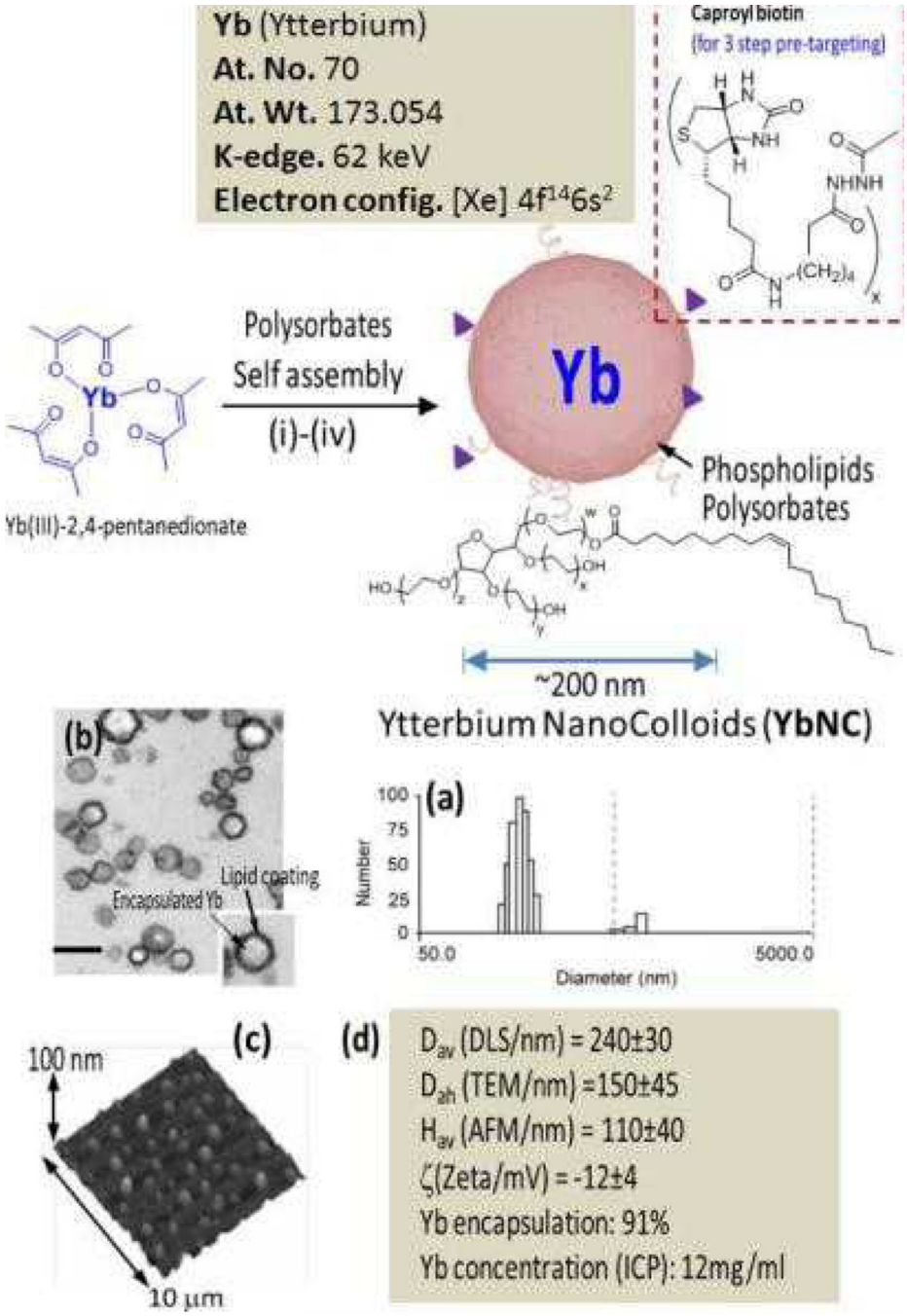

Figure 9.

Synthesis and physico-chemical characterization of self-assembled Ytterbium nanocolloids (YbNC). Schematic describing the preparation of Yb-enriched YbNC: (i) Suspension of Yb(III)-2,4-pentanedionate in Polyoxyethylene (20) sorbitan monooleate, vigorously vortex and mixing, filter using cotton bed, vortex; (ii) preparation of phospholipids thin film comprised of egg lecithin PC, (iii) resuspension of the thin film in water (0.2 µM); (iv) microfluidization at 4°C, 20,000 psi (141 MPa), 4 min, dialysis (cellulosic membrane, MWCO 20K).; characterization table for a representative preparation of YbNC.; (a)

Number-averaged hydrodynamic diameter distribution of YbNC; (b) TEM images of the lipid-encapsulated nanocolloids; (c) AFM image of YbNC drop deposited over glass grid; (d) Physico-chemical characterization chart.

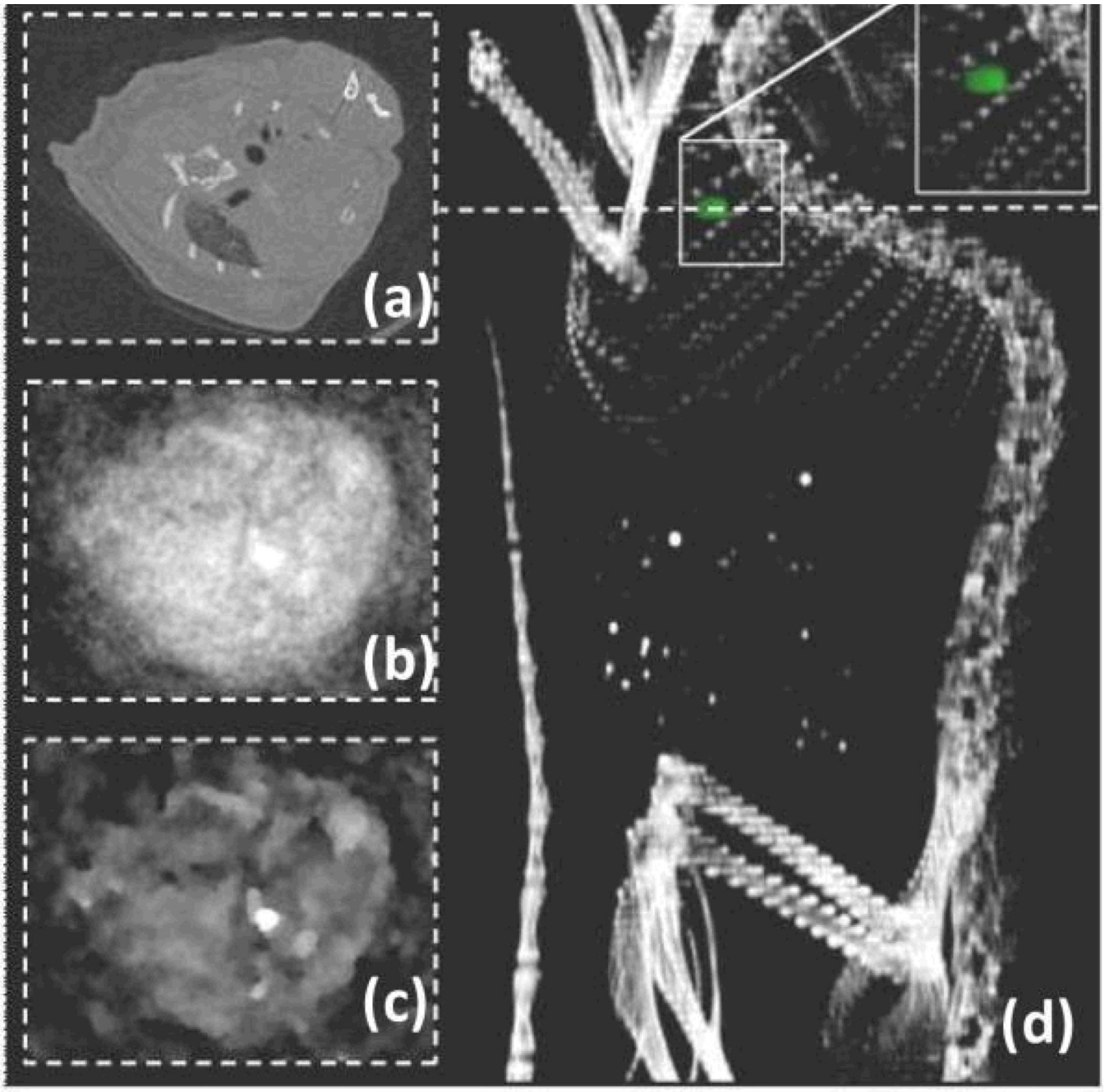

Figure 10.

Blood pool imaging in mouse after bolus application of nontargeted Yb nanocolloids (6ml/kg). (a) Pseudo-conventional CT image composed from spectral measurements, slice through heart (dashed line). Statistical image reconstruction of Yb signal after 1 (b) and 20 iterations. (c) The volume rendered conventional CT image with super positioned Yb signal (green) shows accumulation of Yb in the heart and the clear separation from bone (d).